American Society of Hematology
2021 L Street NW, Suite 900,
Washington, DC 20036
Phone: 202-776-0544 | Fax 202-776-0545
editorial@hematology.org

# Loss of GABARAP mediates resistance to immunogenic chemotherapy in multiple myeloma

Tracking no: BLD-2023-022777R1

Annamaria Gulla (Candiolo Cancer Isntitute FPO-IRCCS, Italy) Eugenio Morelli (Dana Farber Cancer Institute, United States) Megan Johnstone (Dana Farber Cancer Institute, United States) Marcello Turi (Candiolo Cancer Institute FPO-IRCCS, Italy) Mehmet Samur (Dana-Farber Cancer Institute and Harvard School of Public Health, United States) Cirino Botta ("Annunziata" Hospital, Italy) Selma Cifric (Dana Farber Cancer Institute, United States) Pietro Folino (Dana Farber Cancer Institute, United States) Delaney Vinaixa (Dana-Farber Cancer Institute, United States) Francesca Barello (Candiolo Cancer Institute FPO-IRCCS, Italy) Cole Clericuzio (Northeastern University, United States) Vanessa Favasuli (Dana Farber Cancer Institute, United States) Domenico Maisano (Dana-Farber Cancer Institute, United States) Srikanth Talluri (7VA Boston Healthcare System, United States) Rao Prabhala (VA Boston Healthcare System, United States) Giada Bianchi (Brigham and Women's Hospital, United States) Mariateresa Fulciniti (Dana Farber Cancer Institute, United States) Kenneth Wen (Dana Farber Cancer Institute, United States) Keiji Kurata (Dana-Farber Cancer Institute, United States) Jiye Liu (Dana-Farber Cancer Institute, United States) Johany Penailillo (Dana-Farber Cancer Institute, United States) Alberto Bragoni (Candiolo Cancer Institute FPO-IRCCS, Italy) Anna Sapino (Candiolo Cancer Institute FPO-IRCCS, Italy) Paul Richardson (Dana-Farber Cancer Institute, Harvard Medical School, United States) Dharminder Chauhan (Dana Farber Cancer Institute, United States) Ruben Carrasco (Brigham and Women's Hospital, United States) Teru Hideshima (Dana-Farber Cancer Institute, United States) Nikhil Munshi (VA Boston Healthcare System, United States) Kenneth Anderson (Dana Farber Cancer Institute, United States)

**Abstract:**
Immunogenic cell death (ICD) is a form of cell death by which cancer treatments can induce a clinically relevant anti-tumor immune response in a broad range of cancers. In multiple myeloma (MM), the proteasome inhibitor bortezomib is an ICD inducer and creates durable therapeutic responses in patients. However, eventual relapse and resistance to bortezomib appear inevitable. Here, by integrating patient transcriptomic data with an analysis of calreticulin (CRT) protein interactors, we found that GABARAP is a key player whose loss prevented tumor cell death from being perceived as immunogenic after bortezomib treatment. GABARAP is located on chromosome 17p, which is commonly deleted in high-risk MM patients. GABARAP deletion impaired the exposure of the eat-me signal CRT on the surface of dying MM cells in vitro and in vivo, thus reducing tumor cell phagocytosis by dendritic cells and the subsequent anti-tumor T cell response. Low GABARAP was independently associated with shorter MM patient survival and reduced tumor immune infiltration. Mechanistically, we found that GABARAP deletion blocked ICD signaling by decreasing autophagy and altering Golgi apparatus morphology, with consequent defects in the downstream vesicular transport of CRT. Conversely, upregulating autophagy using rapamycin restored Golgi morphology, CRT exposure and ICD signaling in GABARAPKO cells undergoing bortezomib treatment. Therefore, coupling an ICD inducer, like bortezomib, with an autophagy inducer, like rapamycin, may improve patient outcomes in MM, where low GABARAP in the form of del(17p) is common and leads to worse outcomes.

**Conflict of interest:** COI declared - see note

**COI notes:** Conflict-of-interest disclosure: N.C.M. serves on advisory boards of and as consultant to Takeda, BMS, Celgene, Janssen, Amgen, AbbVie, Oncopep, Karyopharm, Adaptive Biotechnology, and Novartis and holds equity ownership in Oncopep. K.C.A. is a consultant of Janssen, Pfizer and Astrazeneca; serves as board member with equity ownership in Oncopep, C4Therapeutics, Starton, NextRNA, Window and Dynamic Cell Therapies. A.G. and K.C.A filed a provisional patent on the role of GABARAP as modulator of ICD. D.C. reports other support from Stemline Therapeutics, Oncopeptides, and C4 Therapeutics outside the submitted work. The remaining authors declare no competing financial interests.

**Preprint server:** No;

**Author contributions and disclosures**: Contribution: A.G. and K.C.A. conceived and designed the research studies; A.G., E.M., and K.C.A. wrote the manuscript; M.T., M.K.S., and C.B. performed in silico analysis of transcriptomic data; A.G., M.J., M.T., and S.C. generated DCs, performed T cell experiments and flow cytometry analysis; P.F. performed microscopy experiments; M.J. and P.F. performed co-ip experiments; S.T. generated MM cells expressing Cas9; E.M., M.J., S.C., P.F., D.V., F.B., C.C., R.P., G.B., M.F., K.W., K.K., J.L., P.G.R., D.C., T.H., N.C.M. contributed to the design, execution, and interpretation of key experiments; V.K.F., D.M, P.F., A.G., and E.M. performed the in vivo study; J.P. and R.D.C. performed the IHC staining of patient samples; A.B. performed the analysis of the IHC staining; and A.S. supervised the IHC analysis.

**Non-author contributions and disclosures**: No;

**Agreement to Share Publication-Related Data and Data Sharing Statement**: Data will be available according to Blood policy.

**Clinical trial registration information (if any)**:

# Loss of GABARAP mediates resistance to immunogenic chemotherapy in multiple myeloma

Annamaria Gulla'[1,2]*, Eugenio Morelli[2,1‡], Megan Johnstone[2‡], Marcello Turi[1‡], Mehmet K. Samur[2,3,4], Cirino Botta[5], Selma Cifric[2], Pietro Folino[2], Delaney Vinaixa[2,6], Francesca Barello[1], Cole Clericuzio[2,6], Vanessa Katia Favasuli[2], Domenico Maisano[2], Srikanth Talluri[2,7], Rao Prabhala[2,7], Giada Bianchi[8], Mariateresa Fulciniti[2], Kenneth Wen[2], Keiji Kurata[2,9], Jiye Liu [2], Johany Penailillo[10], Alberto Bragoni[1,11], Anna Sapino[1,11], Paul G. Richardson[2], Dharminder Chauhan[2], Ruben D. Carrasco[10,12], Teru Hideshima[2], Nikhil C. Munshi[2,7] and Kenneth C. Anderson[2]*

[1]Candiolo Cancer Institute, FPO-IRCCS – Candiolo (TO) 10060, Italy; [2]Department of Medical Oncology, Dana Farber Cancer Institute, Harvard Medical School, Boston, MA; [3]Department of Data Sciences, Dana Farber Cancer Institute, Boston, MA; [4]Department of Biostatistics, Harvard T.H. Chan School of Public Health, Boston, MA; [5]Department of Oncohematology, "Annunziata" Hospital, Cosenza, Italy; [6] Northeastern University, Boston, MA 02115, USA; [7]VA Boston Healthcare System, Boston, MA;[8]Division of Hematology, Department of Medicine, Brigham and Women's Hospital, Harvard medical School, Boston, MA; [9]Division of Medical Oncology/Hematology, Department of Medicine, Kobe University Graduate School of Medicine, Kobe, Japan; [10]Department of Oncologic Pathology, Dana-Farber Cancer Institute, Harvard Medical School, Boston, MA; [11]Department of Medical Sciences, University of Turin, Turin, Italy, [12]Department of Pathology, Brigham and Women's Hospital, Harvard Medical School, Boston.

***Corresponding authors**: Annamaria Gulla, Candiolo Cancer Institute, FPO-IRCCS, Strada Provinciale 142, km. 3.95, 10060 Candiolo (TO) Phone: 011-9933206; E-mail: annamaria.gulla@ircc.it; Kenneth C. Anderson, Dana-Farber Cancer Institute, 450 Brookline Avenue, Boston, MA 02215. Phone: 617-632-2144; Fax: 617-632-2140; E-mail: kenneth_anderson@dfci.harvard.edu.

‡: These authors have equally contributed.

Data are available from the corresponding authors on request according to *Blood* policy.

**Text word count:** 4221

**Abstract word count:** 238

**Number of figures:** 6

**Number of references:** 82

## Key points

- Loss of GABARAP abrogates the surface exposure of calreticulin in dying cancer cells, thus reducing anti-MM immune response after bortezomib.
- Immunogenicity can be restored by combining bortezomib with an autophagy inducer, providing the framework for their clinical translation.

## Abstract

Immunogenic cell death (ICD) is a form of cell death by which cancer treatments can induce a clinically relevant anti-tumor immune response in a broad range of cancers. In multiple myeloma (MM), the proteasome inhibitor bortezomib is an ICD inducer and creates durable therapeutic responses in patients. However, eventual relapse and resistance to bortezomib appear inevitable. Here, by integrating patient transcriptomic data with an analysis of calreticulin (CRT) protein interactors, we found that *GABARAP* is a key player whose loss prevented tumor cell death from being perceived as immunogenic after bortezomib treatment. *GABARAP* is located on chromosome 17p, which is commonly deleted in high-risk MM patients. *GABARAP* deletion impaired the exposure of the eat-me signal CRT on the surface of dying MM cells *in vitro* and *in vivo*, thus reducing tumor cell phagocytosis by dendritic cells and the subsequent anti-tumor T cell response. Low *GABARAP* was independently associated with shorter MM patient survival and reduced tumor immune infiltration. Mechanistically, we found that *GABARAP* deletion blocked ICD signaling by decreasing autophagy and altering Golgi apparatus morphology, with consequent defects in the downstream vesicular transport of CRT. Conversely, upregulating autophagy using rapamycin restored Golgi morphology, CRT exposure and ICD signaling in *GABARAP*$^{KO}$ cells undergoing bortezomib treatment. Therefore, coupling an ICD inducer, like bortezomib, with an autophagy inducer, like rapamycin, may improve patient outcomes in MM, where low *GABARAP* in the form of del(17p) is common and leads to worse outcomes.

## Introduction

Immunogenic cell death (ICD) is a form of cell death that triggers the release of damage-associated molecular patterns (DAMPs) and other signals that activate the immune system[1,2]. ICD is a critical mechanism by which cancer treatments, such as chemotherapy, radiation therapy, and targeted therapy, can induce an anti-tumor immune response and promote the elimination of cancer cells[2,3]. In fact, ICD is important for treatment efficacy in multiple cancers, including breast[4-7], colon[8,9], lung[10-12] cancer and hematologic neoplasms[13-16].

In general, during ICD, the dying tumor cell will emit specific pro-phagocytic signals, including exposing the endoplasmic reticulum (ER) protein calreticulin (CRT) on the cell surface[2,3,17-19]. Exposure of this 'eat me' signal promotes the phagocytosis of tumor cells by antigen-presenting cells (APCs), such as dendritic cells (DCs) and macrophages[17,18,20], which process and present the tumor antigens to T cells[20,21], thus initiating an adaptive anti-tumor immune response[2,3,22,23]. However, cancer cells can exploit several pathways to subvert the induction of ICD[3,24,25], and the exact mechanisms they use and how to combat those mechanisms remain open questions.

Multiple myeloma (MM) is an incurable malignancy of the plasma cells that accounts for ~10% of hematologic cancers[26]. It is characterized by dysfunction of the immune system, particularly of anti-MM immunity, over the course of the disease[27-29]. As such, immunogenic chemotherapy stands out as an ideal therapeutic opportunity to restore endogenous T-cell competence in MM. In fact, the clinical success of the standard-of-care drug bortezomib (BTZ) significantly relies on its ability to kill MM cells in an immunogenic fashion, thus rendering them beacons to the immune system[30-34]. BTZ stimulates the exposure of CRT on the dying cell surface, which stimulates an anti-tumor response[30]. Yet, MM patients inevitably become resistant to BTZ and relapse. We believe this suggests that tumor cells may develop resistance not only to the process of cell death but more precisely to its immunogenic consequences. Therefore, we integrated transcriptomic and proteomic data to identify genes that affect the exposure

of CRT, thus potentially causing resistance to immunogenic chemotherapy. We found that losing GABA Type A Receptor-Associated Protein, GABARAP, a well-known regulator of autophagy and vesicular trafficking[35,36], two processes that are important for CRT exposure and ICD[19,37,38], is a novel mechanism of tumor escape from phagocytosis that contributes to resistance and poor clinical outcomes. Our findings suggest that clinical response can be restored using autophagy inducers.

## Methods

### Cell lines and drugs

Cell lines were grown at 37°C at 5% $CO_2$. Detailed information on cell lines and drugs are included in Supplementary Methods.

### Peripheral blood mononuclear cells

Healthy donor peripheral blood mononuclear cells (PBMCs) were obtained after written informed consent approved by the Institutional Review Board of the Dana-Farber Cancer Institute. PBMCs were separated by Ficoll-hypaque method (Lonza Group Ltd.)

### Fluorescence protein detection, immunofluorescence analysis of protein co-localization and Golgi area

Detailed information about the protocol and list of antibodies are included as Supplementary Methods.

### CRISPR/Cas9 gene knockout and stable gene expression

CRISPR/Cas9 gene knockout or stable gene expression was generated as previously described[30,39]. Detailed information on the protocol and sgRNA sequences can be found in Supplementary Methods.

### Co-immunoprecipitation (Co-IP), immunoblotting and proteomic analysis

Coimmunoprecipitation was performed using the Pierce™ Co-Immunoprecipitation Kit (ThermoFisher Scientific, cat# 26149). Detailed information on the procedures, list of antibodies and proteomic analysis can be found in Supplementary Methods.

**Proximity labeling assay**

AMO1, H929 and U266 cell lines were transduced with CRT-3xHA-TurboID or 3xHA-TurboID doxycycline-inducible expressing vector as previously described. The cDNA sequence coding for Turbo-ID-3xHA[40] or the CRT (NM_004343)-3xHA-TurboID sequence was synthesized and cloned into the pLVX-Tet-One-Puro inducible expression system[41] from Azenta (Azenta US, Inc). Detailed information on the assay can be found in Supplementary Methods.

**Analysis of apoptosis and ATP release**

Detailed information on these procedures is included in Supplementary Methods.

**Generation of monocyte-derived DCs and phagocytosis assay**

Generation of monocyte-derived DCs and phagocytosis assay was performed as previously described[30]. Detailed information on these procedures can be found in Supplementary Methods.

**T cell cytotoxicity assay**

T cell cytotoxicity assay was performed as previously described[30]. A detailed description of the procedure is included in Supplementary Methods.

**Transmission Electron microscopy (TEM) and immunohistochemistry analysis**

A detailed description of sample preparation and analysis is included in Supplementary Methods.

**In vivo studies**

6-week-old female immunocompetent C57BL/KaLwRijHsd (Envigo) mice were housed in the animal facility at DFCI. All experiments were performed after approval by the Animal Ethics Committee of the DFCI and performed using institutional guidelines. Detailed information can be found in Supplementary Methods.

## RNAseq data of MM patients

We used RNAseq from a previously published dataset of newly diagnosed clinically annotated MM patients from the IFM/DFCI 2009 clinical trial[42]. After QC controls, all RNAseq data were quantified with Salmon. Raw counts and TPM values were summed to gene levels using tximport, and DESeq2 was used for all differential gene expression analyses. All figures were created with R and ggplot2. Survival analysis was performed using the survival package in R, and the log-rank test was used to compare groups.

## Analysis of RNAseq and Single Cell RNAseq datasets

Analysis of publicly available RNAseq and single-cell RNAseq datasets is detailed in Supplementary Methods. Single-cell data from NBM (*n*=15), MGUS (*n*=19), SMM (*n*=10), NDMM (*n*=17) and RRMM (pre-therapy) (*n*=19) patients were retrieved from GSE145977, GSE124310[43], GSE161801[44] and GSE163278[45] datasets.

## Statistical Analysis

Statistical significance of differences was determined using the Student t-test (unless otherwise specified for comparison of more than two groups), with the minimal level of significance specified as $p<0.05$. Kaplan-Meier survival curves were compared by log-rank test. All statistical analyses were performed using GraphPad software (http://www.graphpad.com).

Approval of your Institutional Review Board or Animal Care and Use Committee have been obtained for the studies.

## Results

## GABARAP is a clinically relevant binding partner of CRT

We first identified CRT's binding partners by performing mass spectrometry analysis on CRT-bound proteins in AMO1 MM cells. This analysis was performed before and after treatment with BTZ (**Table 1**), which induces ICD and CRT exposure in this specific cell line[30]. To find proteins that potentially drive CRT exposure, we focused on the proteins enriched post-BTZ treatment. Within these proteins, gene-ontology analysis found an enrichment in proteins involved in Golgi transport vesicles and membrane protein complexes, consistent with the vesicular transport of CRT to the plasma membrane (FDR<1%) (**Supplementary Fig. S1A and Table 2)**. To focus on the clinically relevant interactors, we integrated these results with the transcriptomic analysis of MM patients. We interrogated RNA-seq data from newly diagnosed, uniformly treated, and clinically annotated MM patients (IFM/DFCI 2009, NCT01191060)[42] for a list of genes differentially expressed among MM patients with longer survival (>5 years) vs poor survival (<1.5 years) after BTZ-based treatment (p value <0.01) (**Supplementary Fig. S1B**). By combining these two analyses, we found that GABA Type A Receptor-Associated Protein *(GABARAP)* and carnitine palmitoyl transferase 1A (*CPT1A)* were both binding partners of CRT during the ICD process and had lower expression in patients with worse clinical outcome (**Fig. 1A**).

For confirmation, we tested the association of GABARAP and CPT1A to clinical outcome in the IFM/DFCI dataset and two additional independent datasets (GSE9782; GSE4581)[46] using a conventional linear regression model. We found that low expression of *GABARAP,* but not of *CPT1A,* correlated with inferior clinical outcome in MM patients (**Fig. 1B-C; Supplementary Fig. S1C-D**). Furthermore, the *GABARAP* gene locus is on chr17p13.1, a chromosomal region whose deletion is a high-risk marker in MM patients[47]. Indeed, although *GABARAP* is broadly downregulated in MM patients compared to healthy individuals (**Supplementary Fig. S1E**), its expression among MM patient subgroups is significantly lower in those carrying del(17p) (**Supplementary Fig. S1F**). However, the prognostic significance of *GABARAP* levels was still maintained even after excluding MM patients with del(17p) from the analysis, thus suggesting its independent role as a risk predictor (**Fig. 1D-E**). By interrogating

The Cancer Genome Atlas (TGCA) database (https://www.cancer.gov/tcga)[48-51], we also found that low levels of *GABARAP* were associated with poor clinical outcome in other cancers, including brain lower grade glioma (LGG), kidney renal papillary cell carcinoma (KIRP), mesothelioma (MESO), pancreatic adenocarcinoma (PAAD) and uterine corpus endometrial carcinoma (UCEC) (**Supplementary Fig. S1G**).

To molecularly validate the CRT–GABARAP interaction, we immunoprecipitated CRT in cells treated or untreated with BTZ. This experiment confirmed a GABARAP-CRT protein interaction and its increase upon BTZ treatment (**Fig. 1F**). Interaction with another LC3 protein, LC3B, previously reported to interact with CRT[52], was not observed (**Supplementary Fig. S1H**). Treatment with another proteasome inhibitor, Carfilzomib (CFZ), which is also an ICD inducer[53,54], confirmed GABARAP-CRT but not LC3B interaction (**Fig. 1G**; **Supplementary Fig. S1I**). Induction of ER stress by tunicamycin treatment (8 hours) didn't produce a CRT-GABARAP interaction, while it confirmed the CRT-LC3B interaction (**Supplementary Fig. S1J**). These findings were confirmed by confocal microscopy, by which we found that BTZ treatment triggered the colocalization of GABARAP and CRT (**Fig. 1H**).

To validate these findings in living cells, we used the ultra-fast TurboID-based proximity labeling assay[40] (**Supplementary Fig. S1K**). We generated a C-terminally fused CRT-3xHA-TurboID doxycycline-inducible Tet-On lentiviral construct (**Supplementary Fig. S1L**). The fusion of 3xHA-TurboID at the C-terminal of CRT mimics a translocation signal by altering the recognition interface of the KDEL sequence, which is an ER retention signal, as shown in the 3D protein structure predicted using AlphaFold and ChimeraX[55-57] (**Supplementary Fig. S1L**). This way, we generated an artificial system in which CRT translocation was induced by doxycycline, independently of BTZ and ER stress. Validation of the CRT-3xHA-TurboID system and subsequent CRT exposure was performed in three MM cell lines: AMO1, H929 and U266 (**Supplementary Fig. S1M-N**). We used this approach to validate GABARAP as an interactor of CRT during the translocation process. As such, AMO1, H929 or U266 CRT-3XHA-TurboID cells were induced or uninduced with doxycycline for 24 hours in the presence of biotin, and western blot analysis of the streptavidin pull-down proteins confirmed the binding of

GABARAP with CRT during the exposure on the surface in all the cell lines (**Fig. 1I**). These results identify GABARAP as a clinically relevant binding partner of CRT and provide the basis for further investigating whether GABARAP levels may interfere with CRT exposure and induction of the ICD process in MM cells.

## Loss of GABARAP abrogates CRT exposure during ICD

We next explored the role of GABARAP in the cell surface exposure of CRT. We treated a panel of 10 MM cell lines with varying concentrations of BTZ to obtain a similar degree of cell death among cell lines. We found a strong positive linear correlation ($r^2$ = 0.62) between the endogenous expression level of GABARAP protein (**Supplementary Fig. S2A**) and the exposure of CRT on the cell surface induced during BTZ-mediated cell death (**Fig. 2A**). To further confirm the above findings, we utilized KMS11 cells, which exhibit undetectable levels of GABARAP and show an absence of CRT exposure after BTZ. Overexpression of *GABARAP* in these cells restored CRT translocation to the cell surface during BTZ treatment (**Fig. 2B** and **Supplementary Fig. S2B**). Conversely, the KO of *GABARAP* in two ICD-sensitive and GABARAP$^{high}$ cell lines, AMO1 and H929 (**Supplementary Fig. S2C-D**), abrogated CRT exposure after BTZ treatment, as assessed by flow cytometry (**Fig. 2C-D**) and fluorescent microscopy of non-permeabilized cells (**Fig. 2E**). Add-back experiments using *GABARAP*$^{OE}$ in the KO clones restored CRT exposure after BTZ, confirming the on-target effect of *GABARAP* loss (**Fig. 2F; Supplementary Fig. S2E**). Importantly, no significant changes in drug-induced cytotoxicity were detected (**Supplementary Fig. S2F**), indicating that this pathway purely affected the immunogenicity of the cell death.

To widen these observations to other tumor contexts and different ICD inducers, we also tested the outcome of *GABARAP* loss in A549 lung cancer cells. We generated A549 *GABARAP*$^{KO}$ cells (**Supplementary Fig. S2G**) and treated them with crizotinib, a drug previously described as an ICD inducer in this tumor context[11]. Interestingly, GABARAP loss decreased CRT exposure after crizotinib treatment (**Supplementary Fig. S2H**). Altogether, these findings support the role of *GABARAP* in mediating CRT exposure during the induction of ICD.

## Loss of *GABARAP* impairs ICD-induced phagocytosis and anti-tumor T cell activation

Given that surface CRT is an “eat-me” signal, we tested whether *GABARAP* KO reduced tumor phagocytosis by DCs. Indeed, *GABARAP* loss impaired DC-mediated phagocytosis of human AMO1, H929, U266 and murine 5TGM1 myeloma cells (**Fig. 3A, Supplementary Fig. S3A-B-C**). Co-treatment of *GABARAP*$^{KO}$ cells with BTZ and recombinant CRT protein (rCRT), which binds directly to the surface of tumor cells, restored DC-mediated phagocytosis, confirming that *GABARAP* loss impairs phagocytosis via inhibition of CRT translocation (**Fig. 3B**). Similarly, overexpression of GABARAP in KMS11 GABARAP$^{low}$ cells increased cell phagocytosis after treatment with BTZ (**Fig. 3C**).

DC phagocytosis promotes T cell priming and tumor cell recognition, so we next tested whether *GABARAP* loss in tumor cells impaired downstream T cell activation. We incubated WT or *GABARAP*$^{KO}$ HLA.A2.1+ U266 cells, in the presence or absence of BTZ, with donor-matched DCs and T cells, in a system previously described to induce T cell activation[30]. After 5 days of culture, T cells isolated from co-cultures with U266 *GABARAP*$^{KO}$ cells lost the ability to recognize and lyse MM cells (**Fig. 3D**). Overall, these data support the role of GABARAP as a modulator of the anti-tumor response after BTZ immunogenic chemotherapy.

## Loss of *GABARAP* impairs autophagy induction and alters Golgi morphology

To molecularly characterize MM cells exhibiting GABARAP loss, we conducted a comprehensive proteomic analysis comparing *GABARAP* WT and KO in AMO1 and H929 cells. We found that *GABARAP* KO altered the expression of 209 proteins in AMO1 cells (126 down- and 83 up-regulated) and of 102 proteins in H929 cells (51 down- and 51 up-regulated) (**Table 3-4**). Gene set enrichment analysis (GSEA) found a negative enrichment (FDR<1% in AMO1 and FDR<25% in H929) in pathways linked to vesicular transport, autophagosome, ER-to-Golgi trafficking, and Golgi composition (**Fig. 4A, Table 5-6**). Given GABARAP’s known role in vesicular transport and autophagy[35,36], we postulated that, in the absence of *GABARAP*, MM cells exhibiting

lower basal autophagy might undergo biological adaptation within organelles crucial for maintaining their proteostasis, including the Golgi apparatus.

To test this hypothesis, we first confirmed the observed changes at proteomic levels by western blot analysis of several proteins involved in the autophagy machinery (LC3B, ATG4B, GABARAPL2, ATG3) and Golgi trafficking and morphology (PAQR11, GODZ, GOSR1 and SORL1) in both AMO1 and H929 WT or *GABARAP*$^{KO}$ cells (**Supplementary Fig. S4A**). To further confirm the outcome of GABARAP KO on autophagy, we performed transmission electron microscopy (TEM) to compare the number of double or multi-layered vesicles in *GABARAP*$^{KO}$ cells (*n*=30 images) or WT cells (*n*=30 images), which showed significantly fewer vesicles in the absence of GABARAP (**Fig. 4B-C**). Furthermore, confocal microscopy analysis of the *cis*-Golgi matrix protein, GM130, showed an increased area of the Golgi apparatus in *GABARAP*$^{KO}$ cells (**Supplementary Fig. S4B**). TEM similarly depicted a more compact or a more dispersed appearance of the apparatus stacks in AMO1 WT and *GABARAP*$^{KO}$, respectively (**Supplementary Fig. S4C**). Protein trafficking of surface proteins, such as CD138 and MHC-I, as well as paraprotein secretion was not significantly altered in *GABARAP*$^{KO}$ conditions (**Supplementary Fig. S4D-E**), suggesting an adaptation of MM cells to this condition and a specific impairment of protein relocation (such as CRT) triggered by specific stimuli (such as ICD).

We then explored the molecular events induced by BTZ treatment in *GABARAP* WT and KO cells. Western blot analysis of LC3B confirmed that *GABARAP*$^{KO}$ impaired BTZ-induced autophagy in AMO1 and 5TGM1 cells (**Fig. 4D, Supplementary Fig. S4F)**. This effect was restored after *GABARAP* add-back (**Fig. 4D**). Consistently, we found that impairment of autophagy induction after BTZ in AMO1 *GABARAP*$^{KO}$ cells was also associated with decreased release of ATP, another autophagy-related immunogenic DAMP, during ICD[38] (**Supplementary Fig. S4G)**. Similarly, BTZ did not induce ATP release in GABARAP-low KMS11 cells, and this release was efficiently restored after GABARAP overexpression (**Supplementary Fig. S4H)**. While we didn't observe higher BTZ cytotoxicity at the concentration used (**Supplementary Fig. S2F**), nor a difference in poly-ubiquitinated protein levels (**Supplementary Fig. S4I**), the induction of ER

stress after drug treatment was slightly higher after GABARAP loss, consistent with lower autophagy induction (**Supplementary Fig. S4I**).

We further confirmed that the impairment of CRT exposure is dependent on compromised ER-Golgi trafficking and vesicular exocytosis of CRT and not on processes that happen before[19]. Specifically, CRT exposure starts with the induction of ER stress. Two drugs that increase ER stress, tautomycin and salubrinal, did not affect CRT exposure when combined with BTZ in *GABARAP*$^{KO}$ cells (**Supplementary Fig. S4J**). In addition, sub-apoptotic cleavage of caspase 8, the following step required for CRT exposure, did not differ between WT and *GABARAP*$^{KO}$ cells (**Supplementary Fig. S4K**). Taken together, these data show that GABARAP loss compromised the vesicular trafficking of CRT by altering autophagy and Golgi morphology.

Since autophagy and Golgi homeostasis are intricately linked[58], we tested whether increasing autophagy by treating AMO1, H929 and U266 *GABARAP*$^{KO}$ cells with the mTOR inhibitor rapamycin[59] could restore Golgi morphology and CRT trafficking. We found, by confocal microscopy analysis of the GM130 protein, that rapamycin reverted Golgi morphology to resemble that of WT cells by decreasing Golgi area and increasing the compactness of the apparatus stacks in all three cell lines (**Fig. 4E-F; Supplementary Fig. S4L**). TEM analysis performed in AMO1 cells further confirmed the effect of rapamycin on autophagy induction and formation of double-layered vesicles in *GABARAP*$^{KO}$ cells (**Fig. 4G**), which was correlated with a decrease in the dispersion of Golgi morphology, with a higher frequency of cells with a more compact Golgi (**Fig. 4H**).

## Treatment with autophagy inducer restores CRT translocation after BTZ and *in vivo* drug efficacy

We then tested whether a clinically active autophagy inducer, rapamycin, in combination with BTZ would restore CRT translocation and DC-mediated phagocytosis of MM cells. We found that the combination efficiently restored CRT exposure in *GABARAP*$^{KO}$ AMO1 cells **(Fig. 5A**) and in GABARAP$^{low}$ KMS11 cells (**Fig. 5B**). Consistently, combined

treatment increased phagocytosis by DCs of AMO1 cells (*GABARAP*$^{KO}$) and GABARAP$^{low}$ KMS11 cells (**Fig. 5C-D**).

To confirm our *in vitro* observations, we performed two different *in vivo* studies using immunocompetent C57BL/KaLwRijHsd mice carrying tumors of murine 5TGM1 cells. In the first one, we aimed to assess the exposure of CRT on tumors retrieved after BTZ treatment (1 mg/kg, 48 hours). Immunofluorescence staining of CRT protein confirmed that BTZ treatment significantly induced CRT exposure only in WT but not in *gabarap*$^{KO}$ tumors (**Fig. 5E, Supplementary Fig. S5A**). However, the signal from CRT-positive cells in *gabarap*$^{KO}$ tumors significantly increased after combining BTZ with rapamycin (4mg/kg, 24 hour) (**Fig. 5E, Supplementary Fig. S5A)**. Consistently, while we confirmed that BTZ induces a significant regression for WT tumors as previously observed[30] (**Supplementary Fig. S5B**), we found that drug efficacy was significantly lower in mice carrying *gabarap*$^{KO}$ tumors (**Fig. 5F**). However, combination with rapamycin significantly increased BTZ efficacy *in vivo* with no sign of overt toxicity (**Fig. 5F**).

## Tumor intrinsic GABARAP correlates with tumor immune infiltration in MM patients

To evaluate the clinical significance of intratumor GABARAP in the context of anti-MM immunity, we analyzed published datasets of single-cell RNAseq (scRNAseq)[43-45] for a total of 80 samples including normal bone marrow (NBM) (*n=15*), monoclonal gammopathy of undetermined significance (MGUS) (*n=19*), smoldering MM (SMM) (*n=10*), MM (*n=17*) and relapsed/refractory MM (RRMM) (*n=19*). First, we focused the analysis on MM cells identified according to the expression of their main markers (*SDC1*, *CD38*, *TNFRSF17*, *GPRC5D*, *FCRL5* and *CD19*) (**Supplementary Fig. S6A**) and assessed their expression of the ICD gene signature[30]. We found that the expression of the ICD signature in malignant plasma cells progressively decreased during the disease course, consistent with a refractory state in which cells become less responsive to immunogenic stimuli (**Fig. 6A**). Intratumor *GABARAP* expression similarly decreased over MM disease evolution (although heterogeneous expression was

observed in the MGUS patient subgroup, **Fig. 6B**) and was significantly correlated with ICD signature expression (**Fig. 6C**). At the single-cell level, the ICD signature was still downregulated in tumor cells over the disease course (**Supplementary Fig. S6B**) and clustered similarly with *GABARAP* expression (**Fig. 6D**). Concordantly, the expression of *GABARAP* and the ICD signature was correlated at the single-cell level (**Supplementary Fig. S6C**); thus, pointing at the likelihood of a similar outcome on poor tumor immunogenicity.

Next, we sought to assess how the immune microenvironment, and specifically the T cell compartment, is modulated in the context of differential intratumoral GABARAP expression. We first identified the immune cell clusters using known markers (**Supplementary Fig. S6D-F**) and singled out the CD8+ T cells for analysis. We found 29 genes differentially expressed between CD8+ T cells from patients with “high” versus “low” intratumor *GABARAP* expression (according to the median as the dichotomizing value) (**Supplementary Fig. S6G**). We found higher *PRF1* and *HOPX* and lower *CD27* and *CD127* expression in CD8+ T cells from patients with high *GABARAP* expression, indicating a more mature, effector phenotype and higher antigen stimulation mediated by CD4+ T cells (**Fig. 6E**). Moreover, the T cells of patients with *GABARAP*$^{high}$ tumors also showed higher expression of the NeoTCR8 signature, which identifies neoantigen-reactive T cells across metastatic human cancers[60] (**Supplementary Fig. S6H**). Furthermore, immunohistochemical analysis of BM specimens from 10 MM patients found that infiltration of CD3+ and CD8+ T cells was significantly higher in GABARAP$^{high}$ patient tumors (**Fig. 6F-G**). Altogether, these results suggest that tumor intrinsic GABARAP levels are associated with markers of ICD and of higher T cell activity, implying that GABARAP may be a determinant of both spontaneous and ICD-mediated anti-tumor immunity.

## Discussion

We have previously reported that BTZ promotes tumor phagocytosis and anti-tumor adaptive immunity through ICD, thus resulting in a clinical benefit for MM patients[30,33].

However, this dependence on ICD suggests an innovative hypothesis whereby resistance to BTZ may be derived not only from resistance to cell death and defective host immunity but also from a cell's death not being immunogenic enough to trigger anti-tumor immunity. Here, we identified GABARAP as an intrinsic regulator of CRT externalization and tumor immunogenicity.

Importantly, the exposure of CRT after immunogenic chemotherapy has been correlated with the clinical outcome of several cancers[61-65], and mechanisms that interfere with this pathway contribute to poor clinical outcome and response to immune therapies[24,65]. Notably, we found that *GABARAP* expression is correlated with the clinical outcome of various cancer types in which ICD induction has been found to be beneficial for patient outcome: ICD signature predicts prognosis in lower grade glioma[66,67] and endometrial cancer[68]; ICD induction is emerging as a promising therapeutic opportunity in mesothelioma[69]; and immunogenic chemo- and radiation-therapies appear to reactivate the immune system in pancreatic cancer[70,71].

The gene locus of *GABARAP* is on chromosome 17p, which is frequently deleted in high-risk MM[47] as well as in other cancer types[72-74]. In the case of MM, no specific mechanisms of BTZ resistance have been ascribed to 17p deletion; however, BTZ treatment in these patients cannot overcome the adverse impact of del(17p) on outcome[75]. Therefore, we propose that GABARAP deletion is a form of primary resistance to BTZ, since BTZ will be less effective in these patients due to an associated lack of spontaneous and ICD-mediated anti-tumor immunity. Although we did not investigate the clinical and biological consequences of GABARAP loss in other tumor types, nor the correlation of GABARAP with the status of del(17p), the prevalence of this deletion in many cancers[72-74], among other chromosome copy number variations[76], prompts future investigation into the role of GABARAP in patients carrying this abnormality in a broad range of cancers.

GABARAP is a well-known regulator of autophagy and vesicular trafficking[35,77]. It also interacts with the GM130 protein[36], and so GABARAP loss has been previously reported to also alter Golgi morphology[78]. A fragmented Golgi can be observed in a

variety of cancers[58] and is associated with tumor proliferation and invasion, drug resistance and reprogramming of the tumor microenvironment[79,80]. As such, while we posit that CRT and GABARAP interact when induction of ER stress is followed by CRT exposure, our data also pinpoint a strong impairment of autophagy in tumor cells with GABARAP loss, which is the cause of a disrupted Golgi trafficking, that, in turn, renders the translocation of CRT to the cell surface unattainable. Therefore, our study establishes that GABARAP null cells cannot expose CRT because of the autophagy and Golgi dysfunction but leaves open the question about the contribution of the GABARAP-CRT interaction in the process; and about the nature of this interaction, whether direct or indirect, as previously reported[81,82]; and about how other proteins, such as GM130, play a role. Moreover, further studies are necessary to elucidate the mechanisms through which cancer cells downregulate GABARAP and whether components of the tumor microenvironment may influence its expression. In addition, our study uncovered significant correlations between GABARAP loss, autophagy, protein trafficking, and immunogenicity, which warrants further investigation to understand the intricate interplay between these processes in plasma cell biology.

Importantly, our research demonstrated that inducing autophagy alongside immunogenic chemotherapy restored CRT exposure in GABARAP$^{low}$ conditions and converted a non-ICD into an immunogenic one. While immunotherapy is an ideal strategy for addressing immunosuppression in cancer, including MM[28], we believe that restoring the tumor intrinsic immunogenicity of GABARAP-low cells first is essential for effective tumor clearance. Our findings provide the rationale for a combination treatment using an ICD inducer, like BTZ, and an autophagy inducer, like rapamycin, in cancer patients with low GABARAP levels, such as those carrying del(17p), to restore anti-tumor immune recognition and long-term disease control. Additional studies are required to assess the effect of the drug combination on immune effectors and regulators, and are necessary to translate this combination into the clinical setting.

## Acknowledgements

The authors gratefully acknowledge the members of their laboratories for technical advice and critical discussions. The authors thank Christina Usher (Dana-Farber Cancer Institute) for editing the manuscript and insightful comments.

This work is supported by NIH/NCI grants SPORE-P50CA100707, P01CA155258 (N.C.M., K.C.A.); by VA Healthcare System grant No. 5I01BX001584 (N.C.M.); by the Paula and Roger Riney Foundation grant (N.C.M., K.C.A.); and by the Sheldon and Miriam Medical Research Foundation (K.C.A.). A.G. is a Fellow of The Leukemia & Lymphoma Society and a Scholar of the American Society of Hematology; she received support from the International Myeloma Society (IMS); she is supported by an Individual Start-UP grant from the Italian Association for Cancer Research (AIRC) (project #27750); a FPRC “5xmille” 2019 Ministry of Health project (IDEE) and a FPRC “5xmille” 2021 Ministry of Health project (EMAGEN-FaBer). E.M. is supported by a Special Fellow grant from The Leukemia & Lymphoma Society, by a Scholar Award from the American Society of Hematology , by an Individual Start-UP grant from the Italian Association for Cancer Research (AIRC) (project #29106), and by a FPRC “5xmille” 2021 Ministry of Health project (EMAGEN-FaBer). C.C. and D.V. are supported by NCI grant# 5R25CA174650. K.C.A. is an American Cancer Society Clinical Research Professor.

The results shown here are in whole or part based upon data generated by the TCGA Research Network: https://www.cancer.gov/tcga.

## Authorship contributions

Contribution: A.G. and K.C.A. conceived and designed the research studies; A.G., E.M., and K.C.A. wrote the manuscript; M.T., M.K.S., and C.B. performed in silico analysis of transcriptomic data; A.G., M.J., M.T., and S.C. generated DCs, performed T cell experiments and flow cytometry analysis; P.F. performed microscopy experiments; M.J. and P.F. performed co-ip experiments; S.T. generated MM cells expressing Cas9; E.M.,

M.J., S.C., P.F., D.V., F.B., C.C., R.P., G.B., M.F., K.W., K.K., J.L., P.G.R., D.C., T.H., N.C.M. contributed to the design, execution, and interpretation of key experiments; V.K.F., D.M, P.F., A.G., and E.M. performed the in vivo study; J.P. and R.D.C. performed the IHC staining of patient samples; A.B. performed the analysis of the IHC staining; and A.S. supervised the IHC analysis.

## Conflict of Interest Disclosures

Conflict-of-interest disclosure: N.C.M. serves on advisory boards of and as consultant to Takeda, BMS, Celgene, Janssen, Amgen, AbbVie, Oncopep, Karyopharm, Adaptive Biotechnology, and Novartis and holds equity ownership in Oncopep. K.C.A. is a consultant of Janssen, Pfizer and Astrazeneca; serves as board member with equity ownership in Oncopep, C4Therapeutics, Starton, NextRNA, Window and Dynamic Cell Therapies. A.G. and K.C.A filed a provisional patent on the role of GABARAP as modulator of ICD. D.C. reports other support from Stemline Therapeutics, Oncopeptides, and C4 Therapeutics outside the submitted work. The remaining authors declare no competing financial interests.

## References


1. Sistigu A, Yamazaki T, Vacchelli E, et al. Cancer cell-autonomous contribution of type I interferon signaling to the efficacy of chemotherapy. *Nat Med*. 2014;20(11):1301-1309.
2. Kroemer G, Galluzzi L, Kepp O, Zitvogel L. Immunogenic cell death in cancer therapy. *Annu Rev Immunol*. 2013;31:51-72.
3. Kroemer G, Galassi C, Zitvogel L, Galluzzi L. Immunogenic cell stress and death. *Nat Immunol*. 2022;23(4):487-500.
4. Casares N, Pequignot MO, Tesniere A, et al. Caspase-dependent immunogenicity of doxorubicin-induced tumor cell death. *J Exp Med*. 2005;202(12):1691-1701.
5. Goel S, DeCristo MJ, Watt AC, et al. CDK4/6 inhibition triggers anti-tumour immunity. *Nature*. 2017;548(7668):471-475.
6. Sequeira GR, Sahores A, Dalotto-Moreno T, et al. Enhanced Antitumor Immunity via Endocrine Therapy Prevents Mammary Tumor Relapse and Increases Immune Checkpoint Blockade Sensitivity. *Cancer Res*. 2021;81(5):1375-1387.
7. Mattarollo SR, Loi S, Duret H, Ma Y, Zitvogel L, Smyth MJ. Pivotal role of innate and adaptive immunity in anthracycline chemotherapy of established tumors. *Cancer Res*. 2011;71(14):4809-4820.
8. Tesniere A, Schlemmer F, Boige V, et al. Immunogenic death of colon cancer cells treated with oxaliplatin. *Oncogene*. 2010;29(4):482-491.
9. Pozzi C, Cuomo A, Spadoni I, et al. The EGFR-specific antibody cetuximab combined with chemotherapy triggers immunogenic cell death. *Nat Med*. 2016;22(6):624-631.
10. Xie W, Forveille S, Iribarren K, et al. Lurbinectedin synergizes with immune checkpoint blockade to generate anticancer immunity. *Oncoimmunology*. 2019;8(11):e1656502.
11. Liu P, Zhao L, Pol J, et al. Crizotinib-induced immunogenic cell death in non-small cell lung cancer. *Nat Commun*. 2019;10(1):1486.
12. Petrazzuolo A, Perez-Lanzon M, Martins I, et al. Pharmacological inhibitors of anaplastic lymphoma kinase (ALK) induce immunogenic cell death through on-target effects. *Cell Death Dis*. 2021;12(8):713.
13. Schiavoni G, Sistigu A, Valentini M, et al. Cyclophosphamide synergizes with type I interferons through systemic dendritic cell reactivation and induction of immunogenic tumor apoptosis. *Cancer Res*. 2011;71(3):768-778.
14. Wang Z, Chen J, Hu J, et al. cGAS/STING axis mediates a topoisomerase II inhibitor-induced tumor immunogenicity. *J Clin Invest*. 2019;129(11):4850-4862.
15. Tatsuno K, Yamazaki T, Hanlon D, et al. Extracorporeal photochemotherapy induces bona fide immunogenic cell death. *Cell Death Dis*. 2019;10(8):578.
16. Zappasodi R, Pupa SM, Ghedini GC, et al. Improved clinical outcome in indolent B-cell lymphoma patients vaccinated with autologous tumor cells experiencing immunogenic death. *Cancer Res*. 2010;70(22):9062-9072.
17. Zitvogel L, Kepp O, Kroemer G. Decoding cell death signals in inflammation and immunity. *Cell*. 2010;140(6):798-804.
18. Obeid M, Tesniere A, Ghiringhelli F, et al. Calreticulin exposure dictates the immunogenicity of cancer cell death. *Nat Med*. 2007;13(1):54-61.

19. Panaretakis T, Kepp O, Brockmeier U, et al. Mechanisms of pre-apoptotic calreticulin exposure in immunogenic cell death. *EMBO J*. 2009;28(5):578-590.
20. Gajewski TF, Schreiber H, Fu YX. Innate and adaptive immune cells in the tumor microenvironment. *Nat Immunol*. 2013;14(10):1014-1022.
21. Galluzzi L, Vitale I, Aaronson SA, et al. Molecular mechanisms of cell death: recommendations of the Nomenclature Committee on Cell Death 2018. *Cell Death Differ*. 2018;25(3):486-541.
22. Galluzzi L, Buque A, Kepp O, Zitvogel L, Kroemer G. Immunogenic cell death in cancer and infectious disease. *Nat Rev Immunol*. 2017;17(2):97-111.
23. Legrand AJ, Konstantinou M, Goode EF, Meier P. The Diversification of Cell Death and Immunity: Memento Mori. *Mol Cell*. 2019;76(2):232-242.
24. Lin H, Kryczek I, Li S, et al. Stanniocalcin 1 is a phagocytosis checkpoint driving tumor immune resistance. *Cancer Cell*. 2021;39(4):480-493 e486.
25. Vacchelli E, Ma Y, Baracco EE, et al. Chemotherapy-induced antitumor immunity requires formyl peptide receptor 1. *Science*. 2015;350(6263):972-978.
26. Gulla A, Anderson KC. Multiple myeloma: the (r)evolution of current therapy and a glance into future. *Haematologica*. 2020;105(10):2358-2367.
27. Sklavenitis-Pistofidis R, Aranha MP, Redd RA, et al. Immune biomarkers of response to immunotherapy in patients with high-risk smoldering myeloma. *Cancer Cell*. 2022;40(11):1358-1373 e1358.
28. Yamamoto L, Amodio N, Gulla A, Anderson KC. Harnessing the Immune System Against Multiple Myeloma: Challenges and Opportunities. *Front Oncol*. 2020;10:606368.
29. Dhodapkar MV. The immune system in multiple myeloma and precursor states: Lessons and implications for immunotherapy and interception. *Am J Hematol*. 2023;98 Suppl 2(Suppl 2):S4-S12.
30. Gulla A, Morelli E, Samur MK, et al. Bortezomib induces anti-multiple myeloma immune response mediated by cGAS/STING pathway activation. *Blood Cancer Discov*. 2021;2(5):468-483.
31. Richardson PG, Sonneveld P, Schuster M, et al. Extended follow-up of a phase 3 trial in relapsed multiple myeloma: final time-to-event results of the APEX trial. *Blood*. 2007;110(10):3557-3560.
32. Richardson PG, Sonneveld P, Schuster MW, et al. Bortezomib or high-dose dexamethasone for relapsed multiple myeloma. *N Engl J Med*. 2005;352(24):2487-2498.
33. Johnstone M, Vinaixa D, Turi M, Morelli E, Anderson KC, Gulla A. Promises and Challenges of Immunogenic Chemotherapy in Multiple Myeloma. *Cells*. 2022;11(16).
34. Spisek R, Charalambous A, Mazumder A, Vesole DH, Jagannath S, Dhodapkar MV. Bortezomib enhances dendritic cell (DC)-mediated induction of immunity to human myeloma via exposure of cell surface heat shock protein 90 on dying tumor cells: therapeutic implications. *Blood*. 2007;109(11):4839-4845.
35. Schaaf MB, Keulers TG, Vooijs MA, Rouschop KM. LC3/GABARAP family proteins: autophagy-(un)related functions. *FASEB J*. 2016;30(12):3961-3978.
36. Joachim J, Jefferies HB, Razi M, et al. Activation of ULK Kinase and Autophagy by GABARAP Trafficking from the Centrosome Is Regulated by WAC and GM130. *Mol Cell*. 2015;60(6):899-913.
37. Li Y, Wang LX, Yang G, Hao F, Urba WJ, Hu HM. Efficient cross-presentation depends on autophagy in tumor cells. *Cancer Res*. 2008;68(17):6889-6895.
38. Michaud M, Martins I, Sukkurwala AQ, et al. Autophagy-dependent anticancer immune responses induced by chemotherapeutic agents in mice. *Science*. 2011;334(6062):1573-1577.
39. Morelli E, Fulciniti M, Samur MK, et al. A MIR17HG-derived long noncoding RNA provides an essential chromatin scaffold for protein interaction and myeloma growth. *Blood*. 2023;141(4):391-405.
40. Branon TC, Bosch JA, Sanchez AD, et al. Efficient proximity labeling in living cells and organisms with TurboID. *Nat Biotechnol*. 2018;36(9):880-887.

41. Axelrod HD, Valkenburg KC, Amend SR, et al. AXL Is a Putative Tumor Suppressor and Dormancy Regulator in Prostate Cancer. *Mol Cancer Res*. 2019;17(2):356-369.
42. Samur MK, Minvielle S, Gulla A, et al. Long intergenic non-coding RNAs have an independent impact on survival in multiple myeloma. *Leukemia*. 2018;32(12):2626-2635.
43. Zavidij O, Haradhvala NJ, Mouhieddine TH, et al. Single-cell RNA sequencing reveals compromised immune microenvironment in precursor stages of multiple myeloma. *Nat Cancer*. 2020;1(5):493-506.
44. Tirier SM, Mallm JP, Steiger S, et al. Subclone-specific microenvironmental impact and drug response in refractory multiple myeloma revealed by single-cell transcriptomics. *Nat Commun*. 2021;12(1):6960.
45. Bailur JK, McCachren SS, Doxie DB, et al. Early alterations in stem-like/resident T cells, innate and myeloid cells in the bone marrow in preneoplastic gammopathy. *JCI Insight*. 2019;5(11).
46. Mulligan G, Mitsiades C, Bryant B, et al. Gene expression profiling and correlation with outcome in clinical trials of the proteasome inhibitor bortezomib. *Blood*. 2007;109(8):3177-3188.
47. Corre J, Perrot A, Caillot D, et al. del(17p) without TP53 mutation confers a poor prognosis in intensively treated newly diagnosed patients with multiple myeloma. *Blood*. 2021;137(9):1192-1195.
48. Bonneville R, Krook MA, Kautto EA, et al. Landscape of Microsatellite Instability Across 39 Cancer Types. *JCO Precis Oncol*. 2017;2017.
49. Uhlen M, Zhang C, Lee S, et al. A pathology atlas of the human cancer transcriptome. *Science*. 2017;357(6352).
50. Cerami E, Gao J, Dogrusoz U, et al. The cBio cancer genomics portal: an open platform for exploring multidimensional cancer genomics data. *Cancer Discov*. 2012;2(5):401-404.
51. Gao J, Aksoy BA, Dogrusoz U, et al. Integrative analysis of complex cancer genomics and clinical profiles using the cBioPortal. *Sci Signal*. 2013;6(269):pl1.
52. Yang Y, Ma F, Liu Z, et al. The ER-localized Ca(2+)-binding protein calreticulin couples ER stress to autophagy by associating with microtubule-associated protein 1A/1B light chain 3. *J Biol Chem*. 2019;294(3):772-782.
53. Jarauta V, Jaime P, Gonzalo O, et al. Inhibition of autophagy with chloroquine potentiates carfilzomib-induced apoptosis in myeloma cells in vitro and in vivo. *Cancer Lett*. 2016;382(1):1-10.
54. Matsushita M, Kashiwazaki S, Kamiko S, et al. Immunomodulatory Effect of Proteasome Inhibitors via the Induction of Immunogenic Cell Death in Myeloma Cells. *Pharmaceuticals (Basel)*. 2023;16(10).
55. Jumper J, Evans R, Pritzel A, et al. Highly accurate protein structure prediction with AlphaFold. *Nature*. 2021;596(7873):583-589.
56. Varadi M, Anyango S, Deshpande M, et al. AlphaFold Protein Structure Database: massively expanding the structural coverage of protein-sequence space with high-accuracy models. *Nucleic Acids Res*. 2022;50(D1):D439-D444.
57. Pettersen EF, Goddard TD, Huang CC, et al. UCSF ChimeraX: Structure visualization for researchers, educators, and developers. *Protein Sci*. 2021;30(1):70-82.
58. Benyair R, Eisenberg-Lerner A, Merbl Y. Maintaining Golgi Homeostasis: A Balancing Act of Two Proteolytic Pathways. *Cells*. 2022;11(5).
59. Stromberg T, Dimberg A, Hammarberg A, et al. Rapamycin sensitizes multiple myeloma cells to apoptosis induced by dexamethasone. *Blood*. 2004;103(8):3138-3147.
60. Lowery FJ, Krishna S, Yossef R, et al. Molecular signatures of antitumor neoantigen-reactive T cells from metastatic human cancers. *Science*. 2022;375(6583):877-884.
61. Fucikova J, Truxova I, Hensler M, et al. Calreticulin exposure by malignant blasts correlates with robust anticancer immunity and improved clinical outcome in AML patients. *Blood*. 2016;128(26):3113-3124.

62. Truxova I, Kasikova L, Salek C, et al. Calreticulin exposure on malignant blasts correlates with improved natural killer cell-mediated cytotoxicity in acute myeloid leukemia patients. *Haematologica*. 2020;105(7):1868-1878.
63. Fucikova J, Becht E, Iribarren K, et al. Calreticulin Expression in Human Non-Small Cell Lung Cancers Correlates with Increased Accumulation of Antitumor Immune Cells and Favorable Prognosis. *Cancer Res*. 2016;76(7):1746-1756.
64. Kasikova L, Hensler M, Truxova I, et al. Calreticulin exposure correlates with robust adaptive antitumor immunity and favorable prognosis in ovarian carcinoma patients. *J Immunother Cancer*. 2019;7(1):312.
65. Song X, Zhou Z, Li H, et al. Pharmacologic Suppression of B7-H4 Glycosylation Restores Antitumor Immunity in Immune-Cold Breast Cancers. *Cancer Discov*. 2020;10(12):1872-1893.
66. Cai J, Hu Y, Ye Z, et al. Immunogenic cell death-related risk signature predicts prognosis and characterizes the tumour microenvironment in lower-grade glioma. *Front Immunol*. 2022;13:1011757.
67. Sun Z, Jiang H, Yan T, Deng G, Chen Q. Identification of Immunogenic Cell Death-Related Signature for Glioma to Predict Survival and Response to Immunotherapy. *Cancers (Basel)*. 2022;14(22).
68. Pan F, Luo Y, Wang L, et al. Identification of immunogenic cell death-associated subtypes and characterization of the tumor microenvironment in endometrial cancer. *J Gene Med*. 2023:e3495.
69. Di Somma S, Iannuzzi CA, Passaro C, et al. The Oncolytic Virus dl922-947 Triggers Immunogenic Cell Death in Mesothelioma and Reduces Xenograft Growth. *Front Oncol*. 2019;9:564.
70. Ye J, Mills BN, Zhao T, et al. Assessing the Magnitude of Immunogenic Cell Death Following Chemotherapy and Irradiation Reveals a New Strategy to Treat Pancreatic Cancer. *Cancer Immunol Res*. 2020;8(1):94-107.
71. Lu J, Liu X, Liao YP, et al. Nano-enabled pancreas cancer immunotherapy using immunogenic cell death and reversing immunosuppression. *Nat Commun*. 2017;8(1):1811.
72. Consortium ITP-CAoWG. Pan-cancer analysis of whole genomes. *Nature*. 2020;578(7793):82-93.
73. Li Y, Roberts ND, Wala JA, et al. Patterns of somatic structural variation in human cancer genomes. *Nature*. 2020;578(7793):112-121.
74. Liu Y, Chen C, Xu Z, et al. Deletions linked to TP53 loss drive cancer through p53-independent mechanisms. *Nature*. 2016;531(7595):471-475.
75. Avet-Loiseau H, Leleu X, Roussel M, et al. Bortezomib plus dexamethasone induction improves outcome of patients with t(4;14) myeloma but not outcome of patients with del(17p). *J Clin Oncol*. 2010;28(30):4630-4634.
76. Chen M, Chen X, Li S, et al. An Epigenetic Mechanism Underlying Chromosome 17p Deletion-Driven Tumorigenesis. *Cancer Discov*. 2021;11(1):194-207.
77. Joachim J, Razi M, Judith D, et al. Centriolar Satellites Control GABARAP Ubiquitination and GABARAP-Mediated Autophagy. *Curr Biol*. 2017;27(14):2123-2136 e2127.
78. Sanwald JL, Dobner J, Simons IM, et al. Lack of GABARAP-Type Proteins Is Accompanied by Altered Golgi Morphology and Surfaceome Composition. *Int J Mol Sci*. 2020;22(1).
79. Farber-Katz SE, Dippold HC, Buschman MD, et al. DNA damage triggers Golgi dispersal via DNA-PK and GOLPH3. *Cell*. 2014;156(3):413-427.
80. Petrosyan A. Onco-Golgi: Is Fragmentation a Gate to Cancer Progression? *Biochem Mol Biol J*. 2015;1(1).
81. Thielmann Y, Weiergraber OH, Mohrluder J, Willbold D. Structural framework of the GABARAP-calreticulin interface--implications for substrate binding to endoplasmic reticulum chaperones. *FEBS J*. 2009;276(4):1140-1152.
82. Mohrluder J, Stangler T, Hoffmann Y, Wiesehan K, Mataruga A, Willbold D. Identification of calreticulin as a ligand of GABARAP by phage display screening of a peptide library. *FEBS J*. 2007;274(21):5543-5555.

## Figure legends

### Fig. 1 GABARAP is a clinically relevant binding partner of CRT

**A.** Schematic representation of the analysis combining proteomic and transcriptomic data. **B-C**. Prognostic relevance (B. overall survival [OS] or C. progression-free survival [PFS]) of low *GABARAP* level estimated in patients enrolled in the IFM/DFCI. P-value was calculated with a log-rank test. **D-E**. Same analysis as in B-C but excluding IFM/DFCI patients carrying 17p deletion. P-value was calculated with a log-rank test. **F-G**. Immunoblot of GABARAP, CRT and GAPDH on total protein lysates or proteins bound to CRT or IgG isotype control in AMO1 cells untreated or treated with BTZ (5 nM, 10 hours) (F) or CFZ (10 nM, 16 hours) (G). **H**. Representative confocal images of co-immunofluorescence of intracellular staining of GABARAP (green) and CRT (red) in AMO1 WT cells untreated or treated with BTZ (5 nM, 10 hours). DAPI was used to stain nuclei. An enlargement of the squared area shows co-localization with yellow fluorescence due to co-localizing signals. Scale bars, 25µm. Enlargement scale bar, 10µm. **I**. Immunoblot of GABARAP, CRT, Streptavidin and GAPDH on total protein lysates and biotin pull-down proteins before and after doxycycline treatment (1µg/ml, 24h) in AMO1, H929 and U266 CRT-3xHA-TurboID cells.

### Fig. 2 Loss of GABARAP abrogates CRT exposure during ICD

**A.** Correlation between CRT exposure and GABARAP protein expression in a panel of 10 MM cell lines. The surface exposure of CRT was determined by flow cytometry on viable cells after 16 hours of treatment of different cell lines, according to their BTZ sensitivity. Fold change of CRT increase was correlated with abundance of GABARAP protein (as shown in Supplementary Fig. S2A). **B**. Analysis of surface CRT exposure in KMS11 WT and *GABARAP*$^{OE}$ after treatment with BTZ (7.5 nM, 16 hours) by flow cytometry of viable cells. **C-D**. (*left*) Effect of BTZ treatment (16 hours) on the exposure

of surface CRT in AMO1 (5 nM) (C) and H929 (2.5 nM) cells (D) both with WT and *GABARAP*$^{KO}$ as assessed by flow cytometry of viable cells. (*right*) Representative overlay histogram of surface CRT fluorescence (MFI) in AMO1 (C) and H929 (D). **E**. Representative images of immunofluorescence staining of surface CRT (red) in non-permeabilized AMO1 WT and *GABARAP*$^{KO}$ before and after treatment with BTZ. DAPI was used to stain nuclei. Scale bars, 10µm. Enlargement pictures of the squared area show CRT exposure on dying cells only in WT condition. Scale bars, 2µm. **F**. Analysis of surface CRT exposure in AMO1 WT, *GABARAP*$^{KO}$ and *GABARAP*$^{KO}$ in which GABARAP was re-expressed (*GABARAP*$^{KO}$ +add-back) after treatment with BTZ (5 nM, 16 hours) by flow cytometry of viable cells. For B-C-D-F: *$P < 0.05$, **$P < 0.01$, *ns*=not significant (Student unpaired t-test).

**Fig. 3 Loss of *GABARAP* impairs ICD-induced phagocytosis and anti-tumor T cell activation**

**A.** For phagocytosis assay, MM cells and DCs were pre-stained with different dyes (either Far-Red or CFSE). Dye–stained AMO1, H929 and 5TGM1 cells either WT or *GABARAP*$^{KO}$ were left untreated or treated with BTZ (5 nM, 2.5 nM, and 7.5 nM respectively) for 16 hours. Then, they were cocultured with dye-stained DCs. Analysis was performed after 4 hours. Shown in the graph is the fold increase in the percentage of double-positive DCs in treated cells as compared with untreated cells, as assessed by flow cytometry. **B**. Phagocytosis assay of BTZ-treated (5 nM, 16 hours) or untreated stained-AMO1 WT, *GABARAP*$^{KO}$, and *GABARAP*$^{KO}$ with the addition of exogenous recombinant CRT (rCRT) cocultured with stained-DCs for 4 hours. Fold increase in the percentage of double-positive DCs in treated cells compared with untreated cells is shown. On the right, representative overlay histograms confirm the exposure of surface CRT in the different conditions, as assessed by flow cytometry. **C.** Phagocytosis assay of BTZ-treated (7.5 nM, 16 hours) or untreated stained KMS11 WT or *GABARAP*$^{OE}$ cocultured with stained DCs for 4 hours. Fold increase in the percentage of double-positive DCs in treated cells compared with untreated cells is shown. **D**. BTZ-treated (16 hours) or untreated U266 either WT or *GABARAP*$^{KO}$ cells were cocultured with HLA-matched DCs and T cells from the same healthy donors. After 5 days, T cells were

765 negatively selected from all four coculture conditions (α. WT untreated; β. WT treated
766 with BTZ, δ. *GABARAP*$^{KO}$ untreated and γ. *GABARAP*$^{KO}$ treated with BTZ) and then
767 cultured for 24 hours with new U266 GFP+ cells at 1:5 target:effector (T:E) ratio,
768 followed by 7-AAD staining and quantification of MM cell lysis by flow cytometry. Shown
769 in the graph is the fold change increase of MM cell lysis induced by the T cells retrieved
770 from the treated conditions versus the untreated ones. For A-D: *P < 0.05, **P < 0.01,
771 ***P < 0.001 (Student unpaired t-test).
772
773 **Fig. 4 Loss of *GABARAP* impairs autophagy induction and alters Golgi**
774 **morphology**
775 **A**. AMO1 and H929 WT and *GABARAP*$^{KO}$ were subjected to proteomic analysis by
776 multiplexed proteomics with mass spectrometry. Shown in panel A is the GSEA Gene
777 Ontology Cellular components (GOCC) that were significantly negatively enriched after
778 *GABARAP* KO. (FDR<1% for AMO1 and FDR <25% for H929). **B-C**. Analysis of
779 autophagy in AMO1 WT and *GABARAP*$^{KO}$ cells by transmission electron microscopy
780 (TEM). (B) Representative TEM images depicting Golgi morphology A=double-layered
781 vesicles. Scale bars, 500nm. (C) Histograms showing the number of double-layered
782 vesicles as determined in a total of *n*=30 images for AMO1 WT and *n*=30 images for
783 AMO1 *GABARAP*$^{KO}$ cells. **D.** AMO1 WT, *GABARAP*$^{KO}$ and *GABARAP*$^{KO}$ in which
784 GABARAP was re-expressed (*GABARAP*$^{KO}$ +add-back) were left untreated or treated
785 with BTZ (5 nM, 16 hours). Immunoblot of GABARAP and LC3A/B is shown. β-actin
786 was used as a loading control. **E**. Representative confocal images of Golgi apparatus
787 stained with GM-130 antibody (green) in AMO1 WT, *GABARAP*$^{KO}$ and *GABARAP*$^{KO}$
788 treated with Rapamycin (50 nM, 24 hours). DAPI was used to label nuclei. This merged
789 figure is also reported as Supplementary Fig. 4L together with the ones of the single
790 channels. Scale bars, 20μm. **F.** Box plot showing the Golgi area (μm2) in the different
791 conditions as determined in a total of n=119 cells per condition for AMO1, n=60 cells
792 per condition for H929 and n=60 cells per condition for U266. **G**. Representative TEM
793 images depicting Golgi morphology in AMO1 WT, *GABARAP*$^{KO}$ and *GABARAP*$^{KO}$
794 treated with rapamycin (50 nM, 24 hours). C=compact; D=dispersed; S=swollen. Scale
795 bars, 500nm. **H.** Histogram showing the percentage of compact, swollen and dispersed

Golgi in each condition. Specifically, n=61 Golgi were visible in 29 TEM images taken in AMO1 WT; n=37 Golgi in 30 TEM images taken in AMO1 *GABARAP*$^{KO}$; n=47 Golgi in 29 TEM images taken in AMO1 *GABARAP*$^{KO}$ treated with rapamycin. For C: **P < 0.01 based on Student unpaired t-test; for F:****P < 0.0001 Kruskal-Wallis test.

**Fig. 5 Treatment with autophagy inducer restores CRT translocation after BTZ and *in vivo* drug efficacy**

**A.** Flow cytometry analysis of CRT exposure of AMO1 WT or *GABARAP*$^{KO}$ untreated or treated with BTZ (4nM, 16h), rapamycin (100nM, 24h) or a combination of both drugs. Fold increase as compared to untreated cells is shown **B.** Fold increase of CRT levels on surface of KMS11 cells untreated or treated with BTZ (6nM, 16h), rapamycin (500nM, 24h) or a combination of both drugs. **C.** Phagocytosis assay of GFP-AMO1 WT or *GABARAP*$^{KO}$ untreated or pre-treated with BTZ (4 nM, 16 hours), rapamycin (100 nM, 24 hours) or a combination of both drugs cocultured with Far red-DCs for 4 hours. Shown is the fold increase of the percentage of double-positive DCs in treated conditions as compared with untreated cells. **D**. Phagocytosis assay of CFSE-stained KMS11 untreated or pre-treated with BTZ (6 nM, 16 hours), rapamycin (500 nM, 24 hours) or a combination of both drugs cocultured with Far red-DCs for 4 hours. Shown is the fold increase of the percentage of double-positive DCs in treated conditions as compared with untreated cells. **E**. 5TGM1 WT or *gabarap*$^{KO}$ were subcutaneously injected in immunocompetent C57BL/KaLwRijHsd mice. When tumors became palpable, mice bearing WT tumors were randomized to receive either BTZ (1 mg/kg) or PBS; while mice bearing *gabarap*$^{KO}$ tumors were randomized to receive: PBS, BTZ (1 mg/kg), rapamycin (4mg/kg) or a combination of both drugs. Tumors were retrieved 48 hours after BTZ treatment or, in the combination group, 48 hours after BTZ and 24 hours after rapamycin. CRT expression was detected by immunofluorescence. (*left*) Representative images of tumors retrieved from the different groups stained with CRT antibody (red). DAPI was used to label nuclei (blue). Scale bars, 100μm (63x magnification). (*right*) Average of cell intensity of CRT signal is shown, as analyzed by the Halo software. The numbers of observations reported are as follow: WT - BTZ (*n*=21 sections from *n*=7 tumors); WT+BTZ (*n*=18 sections from *n*=6 tumors ) ; *GABARAP*$^{KO}$ –

BTZ (*n*=15 sections from *n*=5 tumors); *GABARAP*$^{KO}$ + BTZ (*n*=18 sections from *n*=6 tumors); *GABARAP*$^{KO}$ + RAPA (*n*=9 sections from *n*=3 tumors) and *GABARAP*$^{KO}$ + RAPA + BTZ (*n*=8 sections from *n*=2 tumors); the signal from each section is represented as a dot in the graph. **F.** Fold increase of tumor growth from day 1 (start of treatment) of subcutaneous 5TGM1 *gabarap*$^{KO}$ xenografts in C57BL/KaLwRijHsd mice treated with PBS (*n*=5), BTZ (1 mg/kg twice/week for 2 weeks) (*n*=4), rapamycin (4mg/kg/day for 5 days) (*n*=5) or a combination of both drugs (*n*=6) ± SEM for each group is reported. For A-F: *P < 0.05, **P < 0.01, ***P<0.001 (Student unpaired t test).

**Fig. 6 Tumor intrinsic GABARAP correlates with tumor immune infiltration in MM patients**

**A-B**. Analysis of ICD signature[30](A) and *GABARAP* (B) expression on data aggregated per a total of 80 patients across MM disease stages (n=15 NBM, n=19 MGUS, n=10 SMM, n=17 MM, n=19 RRMM)39-41. **C**. Linear regression of GABARAP with ICD signature expression in the same patient cohort. **D.** Uniform manifold approximation and projection (UMAP) plots of single-cell transcriptomic of n=80 MM patients showing the density of ICD-signature (D) and *GABARAP* (E) expression on MM plasma cells. **E**. Quantification of the expression of selected markers in CD8+ T cells significantly differentially expressed between MM patients with low versus high intratumoral *GABARAP* expression (median as dichotomizing value). **F**. Representative images of hematoxylin and eosin (H&E) and immunohistochemistry (IHC) analysis of GABARAP expression in plasma cells, and CD3 and CD8 staining of T cells from bone marrow biopsies from MM patients. Scale bars, 100 µm. **G**. Statistical analysis of the percentage of CD3+ or CD8+ T cells in n=10 patients with negative (n=5) or positive (n=5) staining for intratumoral GABARAP. For A-B: P values were calculated using Kruskal-Wallis test. For G: *P < 0.05, Student unpaired t test.

Fig. 1

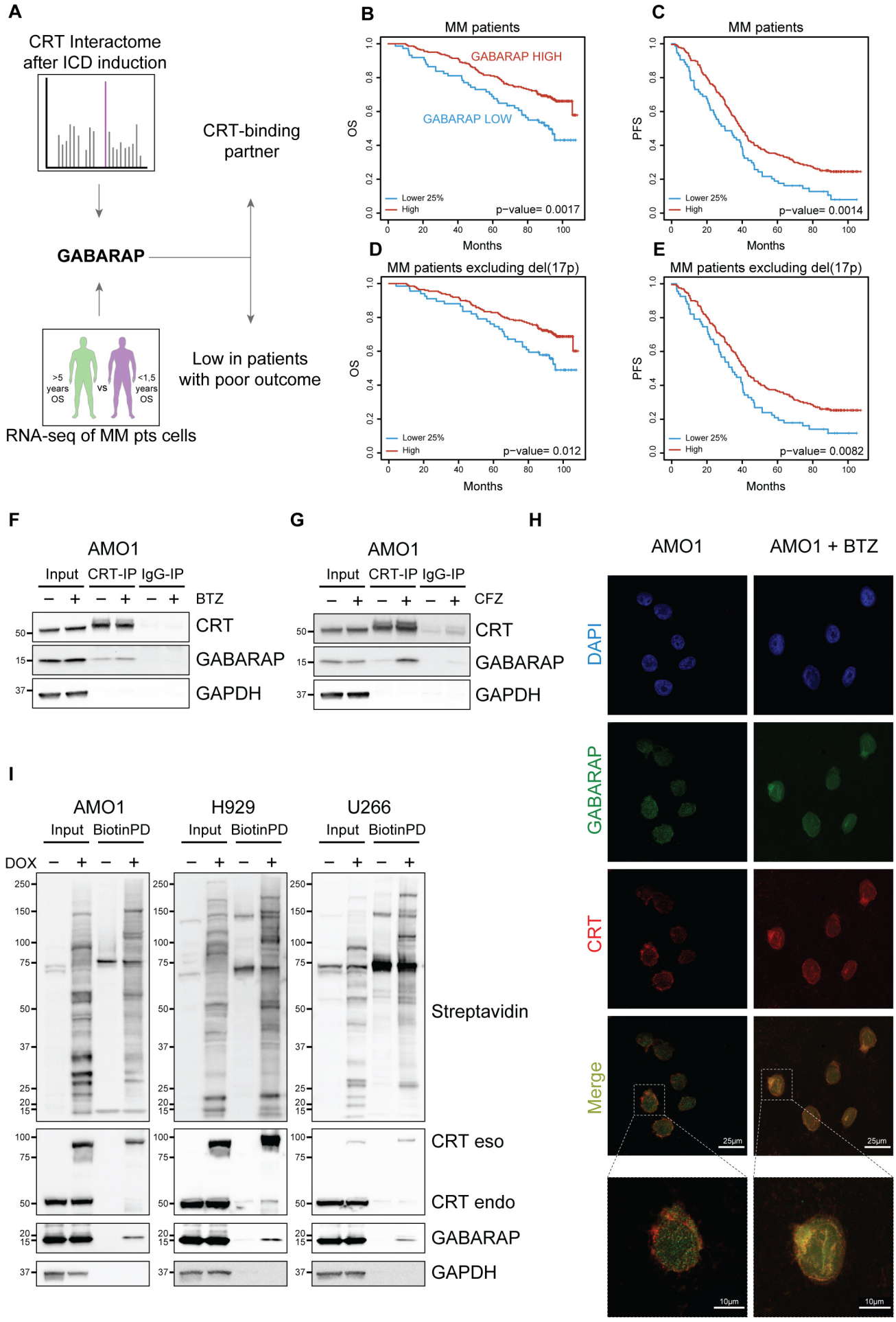

Fig. 2

# Figure 2

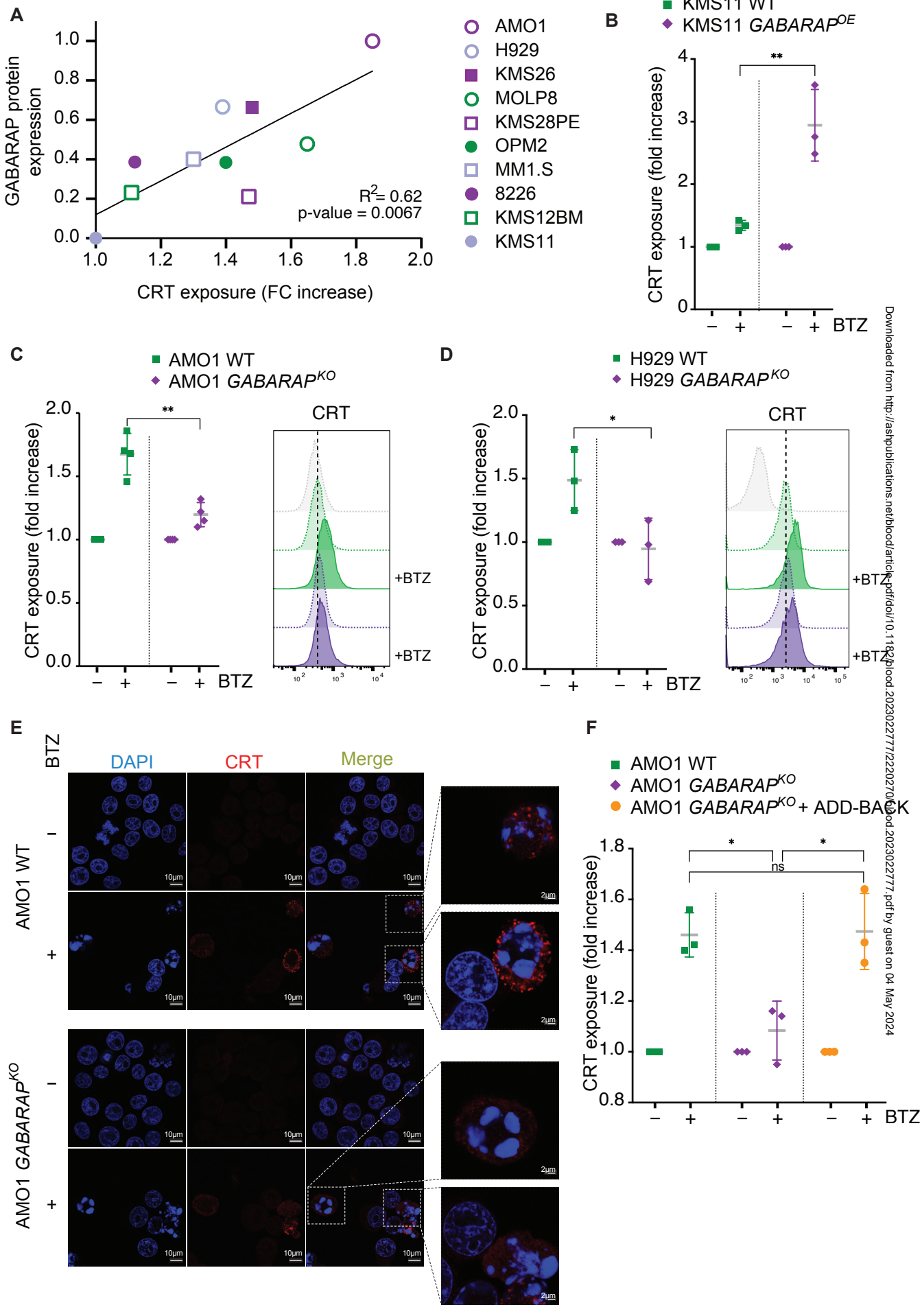

Fig. 3

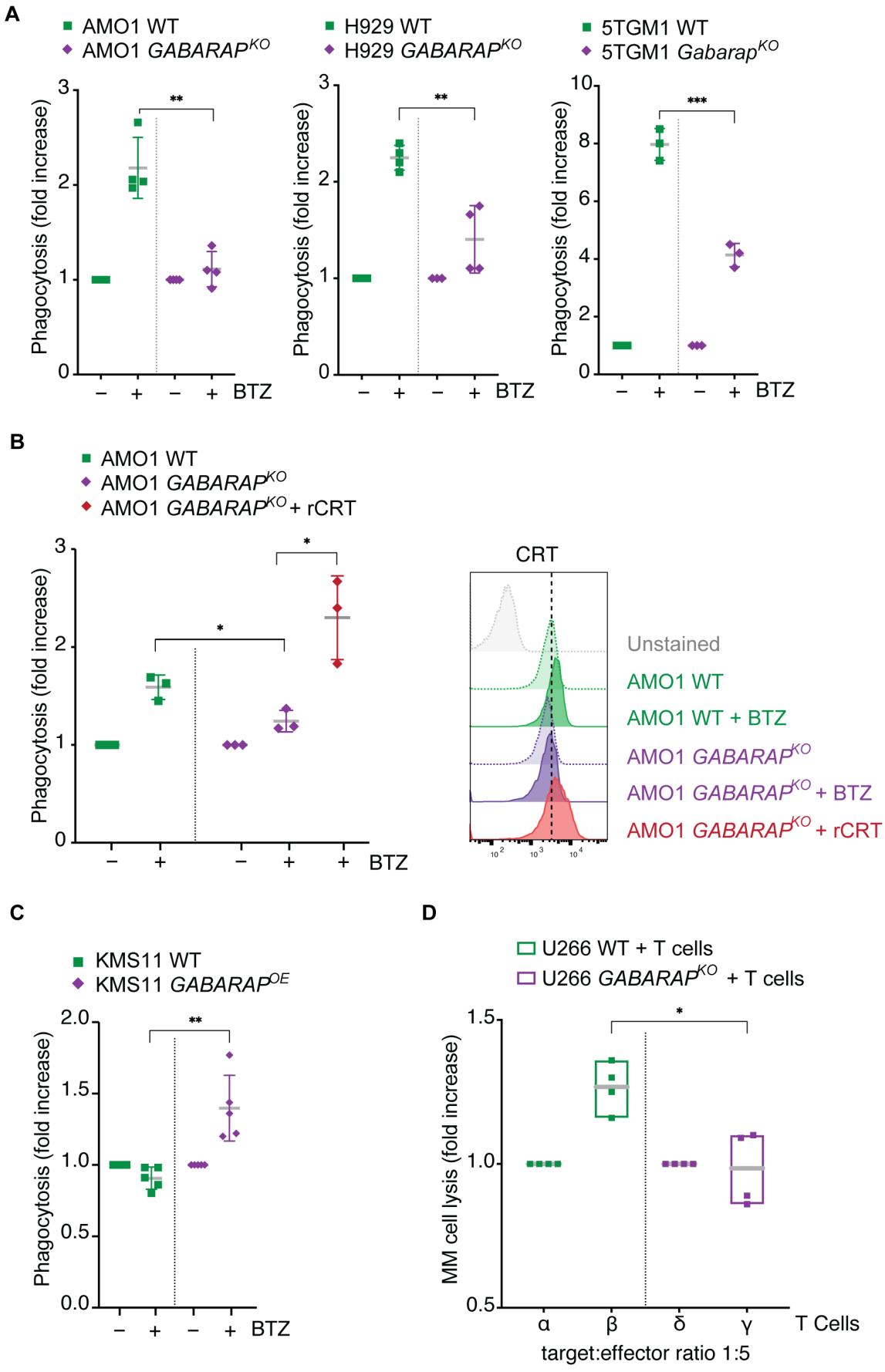

Fig. 4

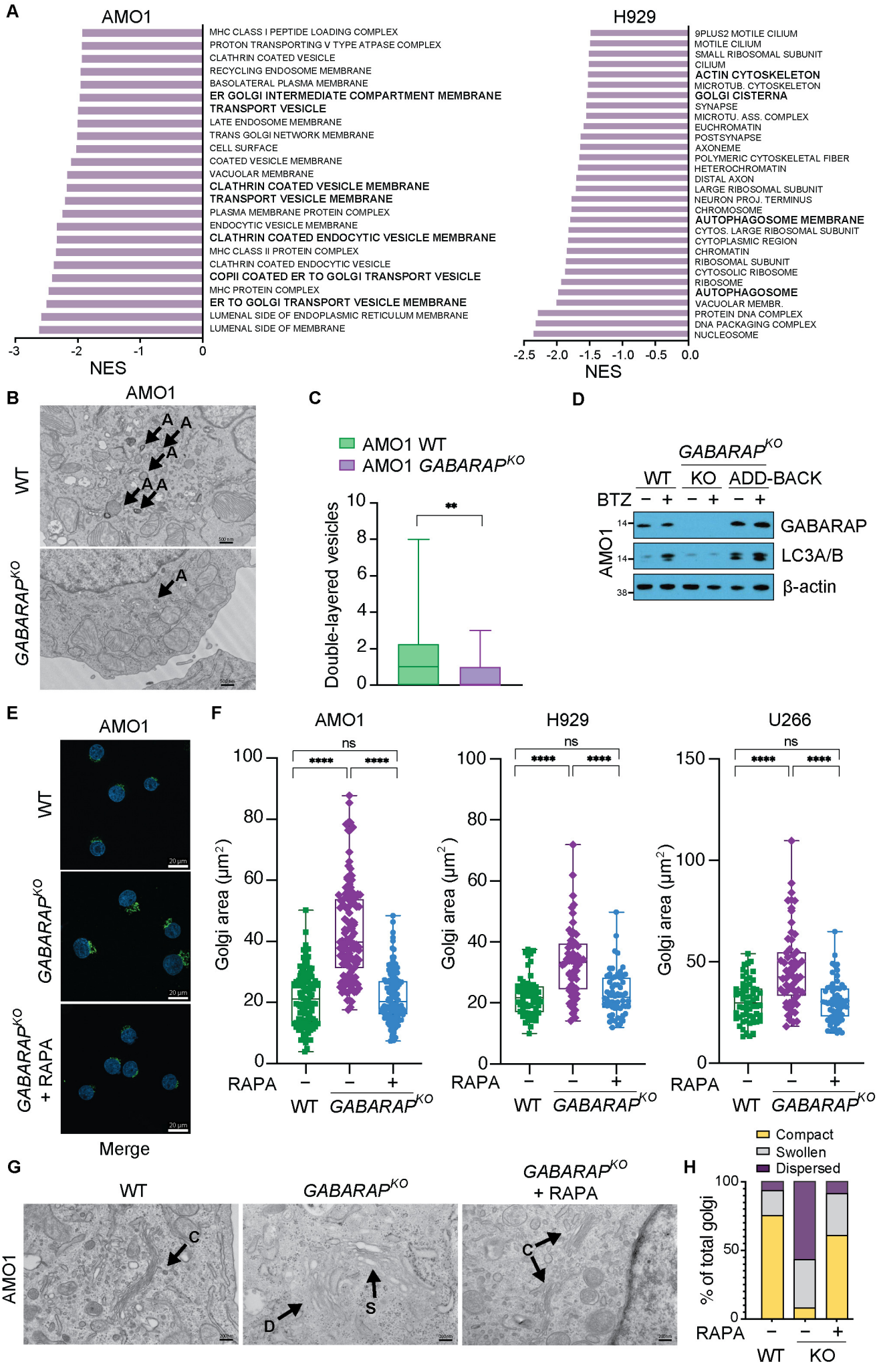

Fig. 5

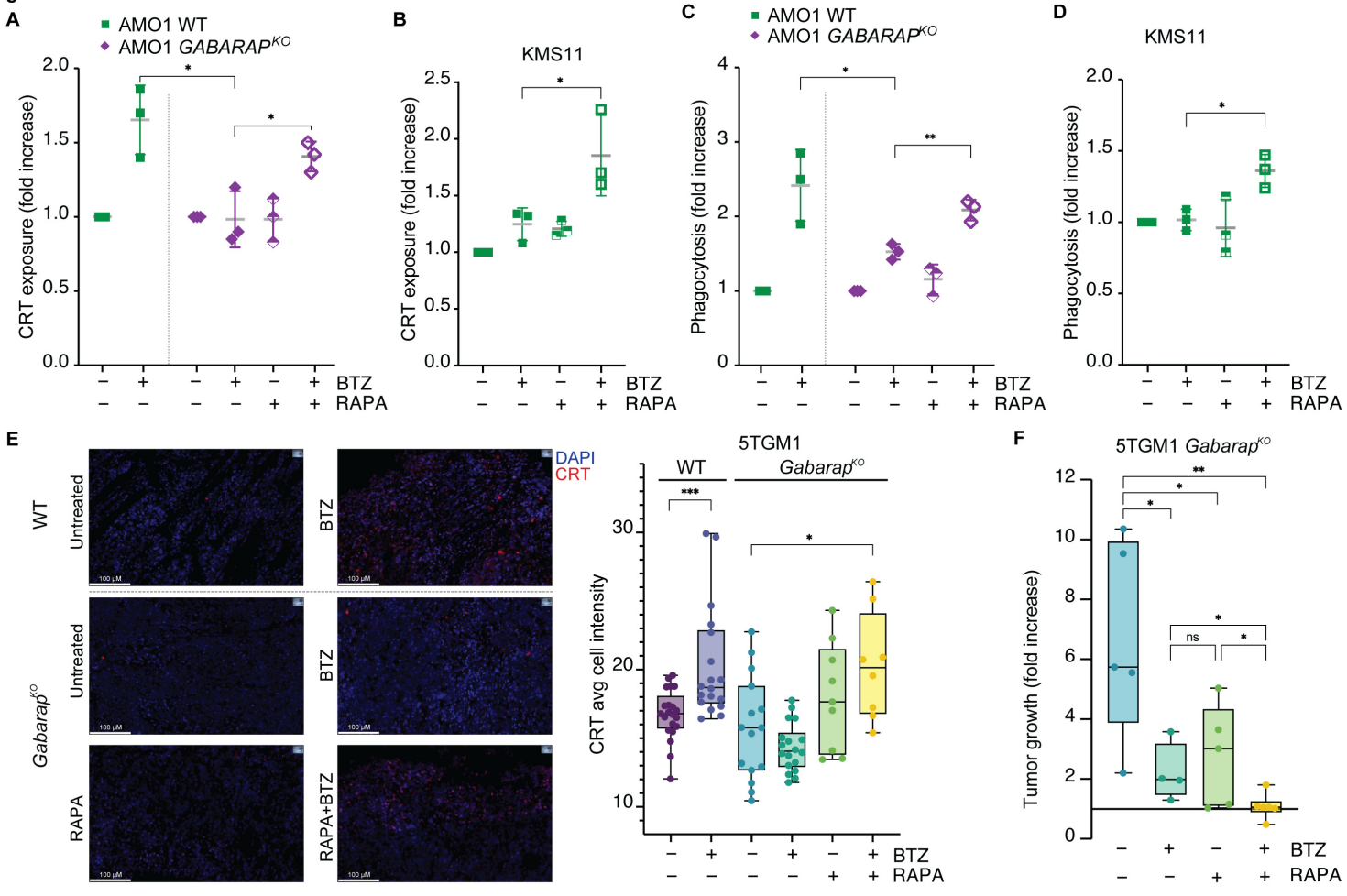

Fig. 6

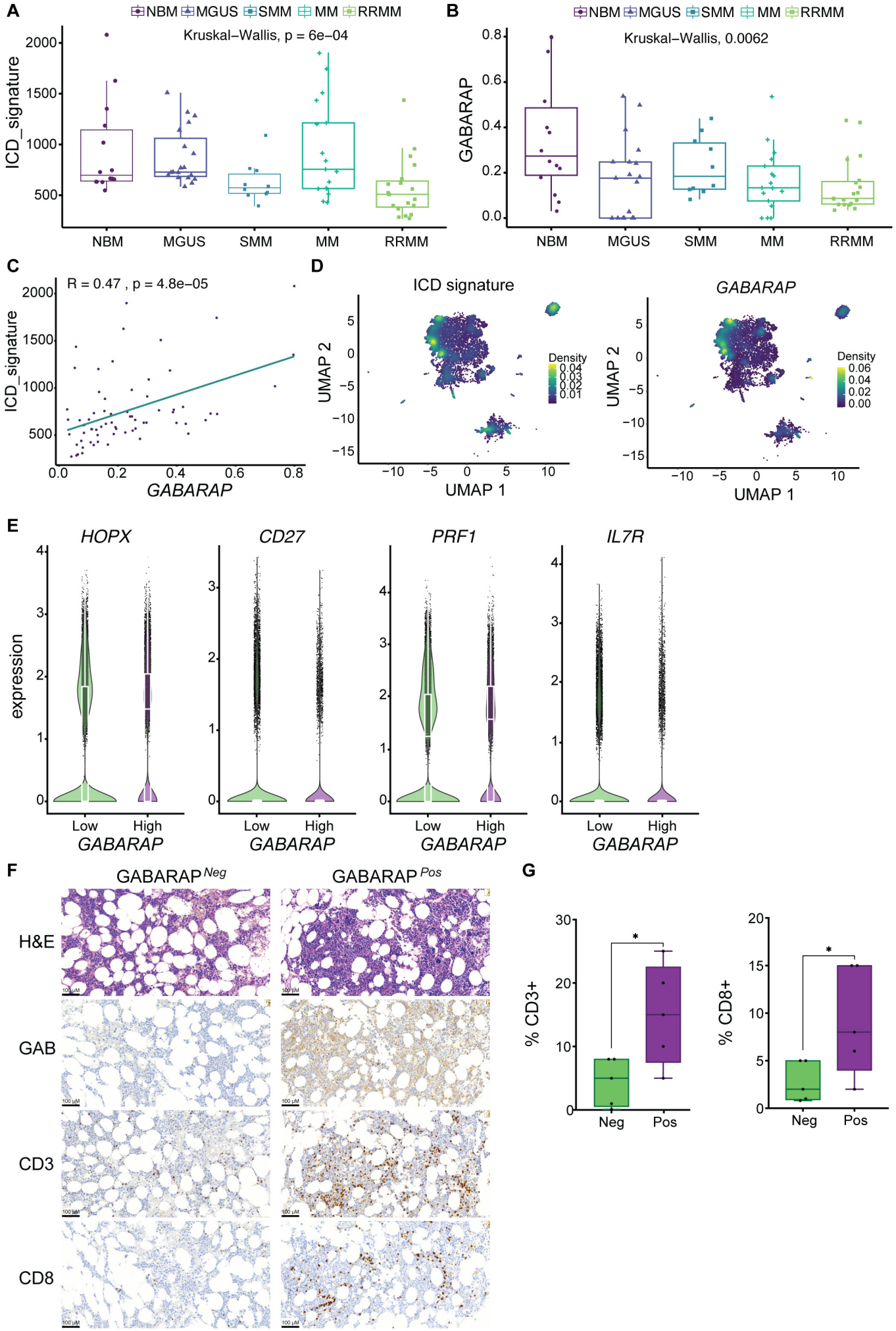

# Role of GABARAP, a Regulator of Autophagy and Vesicular Trafficking, in Immunogenic Cell Death (ICD) in Multiple Myeloma

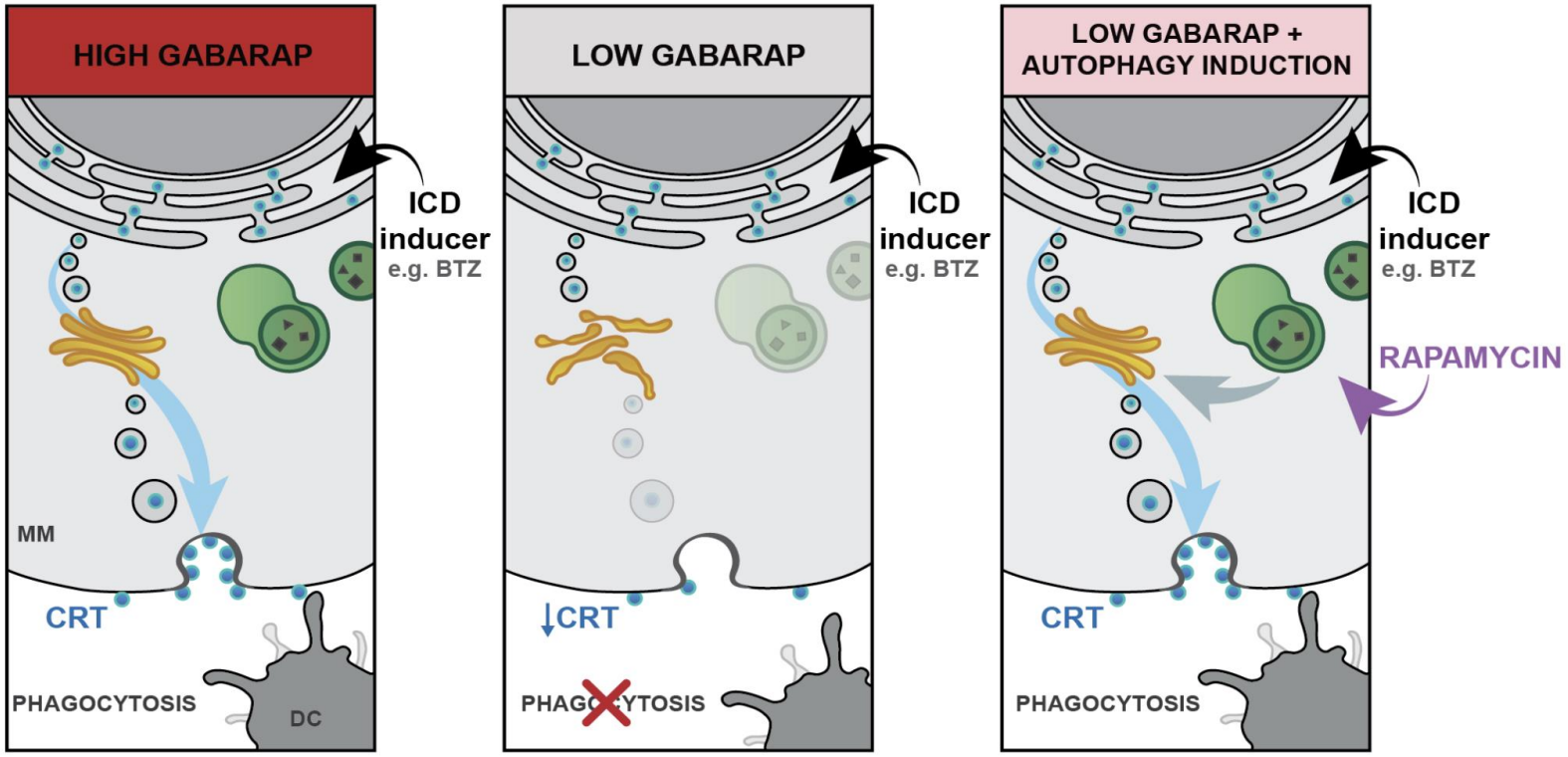


**Conclusions: 1) Loss of GABARAP impairs surface exposure of calreticulin during ICD. 2) Immunogenicity can be restored by combining ICD with an autophagy inducer.**

*Gulla et al. DOI: 10.xxxx/**blood**.2024xxxxxx*

***Blood* Visual Abstract**